JOURNAL OF GEOPHYSICAL RESEARCH, VOL. 92, NO. C10, PAGES 10,787-10,798, SEPTEMBER 15, 1987

TWO-DIMENSIONAL OBSERVATIONS OF TEMPERATURE MICROSTRUCTURE IN A COASTAL REGION

Libe Washburn

Ocean Physics Group, Center for Earth Sciences, University of Southern California, Los Angeles

Abstract. Temperature microstructure is mapped in two dimensions for a section 6.7 km long and 150 m deep in water which is 200 m deep. The section is located on the continental shelf southeast of Point Conception on the southern California coast. Regions of mixing activity are composed of numerous individual events, some of which are observed to collapse onto isopycnal surfaces when plotted in a distance-density coordinate system. Mixing regions with the temperature variance dissipation rate χ exceeding 10^{-6} °C^2 s^{-1} are observed to have isopycnal extents of up to 3 km. Comparison of the distributions of N and χ reveals no consistent relationship between mixing activity and the ambient stratification. Terms in the two-dimensional budget equation for temperature variance $(T')^2$ are compared with χ for a volume bounded by isopycnal surfaces which is about 17 m thick and which spans the data section. The budget for $(T')^2$ is consistent with a balance between diapycnal production and dissipation of $(T')^2$ yielding an effective diapycnal diffusivity of heat of 2.0×10^{-4} m^2 s^{-1}. Water within the averaging volume is thermally stratified and the measured temperature variance dissipation rate may be used to estimate the rate at which kinetic energy is irreversibly lost to mixing of local density gradients. This rate is found to be about 3.3×10^{-8} W kg^{-1} within the averaging volume and is about a factor of 3 smaller than the kinetic energy dissipation rate ϵ typically found in surface mixed layers.

1. Introduction

At present one of the primary methods for determining the vertical turbulent heat flux is that first proposed by Osborn and Cox [1972]. This method is based on a simplified, one-dimensional form of the budget equation for temperature variance $(T')^2$ in which the vertical production of $(T')^2$ averaged over an arbitrary volume is assumed to balance the rate at which $(T')^2$ is destroyed through the combined effects of turbulent shear within mixing events and molecular diffusion. (To simplify notation, $(T')^2$ is used to indicate temperature variance rather than $\langle(T')^2\rangle$, where the angle brackets indicate an averaging procedure.) The production of $(T')^2$ is assumed to result from the occurrence of turbulent overturns in the presence of a mean vertical temperature gradient. Several assumptions are made in applying the simplified production-dissipation balance, including steady state, nondivergence of the vertical and horizontal fluxes of $(T')^2$, and no production of $(T')^2$ due to horizontal mixing processes. A recent discussion of the method is given by Oakey [1982], and further discussion of the pitfalls in applying this simplified balance to oceanic conditions is given by Gargett [1984]. In particular it is pointed out that divergences in the horizontal [Armi, 1979] and vertical [Gargett and Holloway, 1984; Holloway 1983, 1986a, b] fluxes of $(T')^2$ may be important in the $(T')^2$ budget, in which case inferred vertical eddy diffusivities will be overestimates. Gregg et al. [1986] have also recently argued that lateral advective contributions are important in regions containing thermohaline intrusions and that this balance is not applicable. Direct estimates of the vertical heat flux derived from measurements of $\overline{w'T'}$, where w' is a vertical velocity fluctuation, have not yet been made in the ocean because of difficulties in measuring w' to sufficiently small scales.

In this paper the budget equation for $(T')^2$ is considered with respect to a two-dimensional mapping of water properties and temperature microstructure quantities. Mapping of these distributions in two dimensions allows order of magnitude estimates to be made of the possible contributions to the $(T')^2$ budget from advective and isopycnal mixing processes, rather than arbitrarily assuming that these contributions are negligible. The two-dimensional microstructure data are obtained from a tow-yo platform which is moved rapidly in a "sawtooth" pattern to produce as nearly a synoptic picture of mixing activity as possible. However, it is shown that the observed distribution of the temperature variance dissipation rate χ rapidly smooths temperature variance and that significant evolution of the microstructure field probably occurs over the period of observations. Despite this evolution, several regions of microstructure activity are repeatedly encountered on successive profiles, which indicates the presence of laterally coherent mixing regions and indicates that temperature variance is being generated over the course of the observations.

In section 2 the measurement procedures, data analysis, and conditions of the experiment are described. Section 3 is essentially descriptive and contains profiles of χ as a function of both depth and density for the entire data record. These profiles are used to construct contour maps of χ in both pressure-distance and density-distance coordinate systems in an effort to obtain a "snapshot" of the distribution of mixing activity. Density profiles for the entire record are also given along with the water mass characteristics. In section 4 the budget equation for temperature variance is considered for a volume bounded by isopycnal surfaces based on the two-dimensional sampling of temperature, temperature variance, and χ. Advection and production terms are then compared with the observed dissipation rate in order to estimate the dominant balance in the budget equation.

Paper number 7C0516.
0148-0227/87/007C-0516$05.00

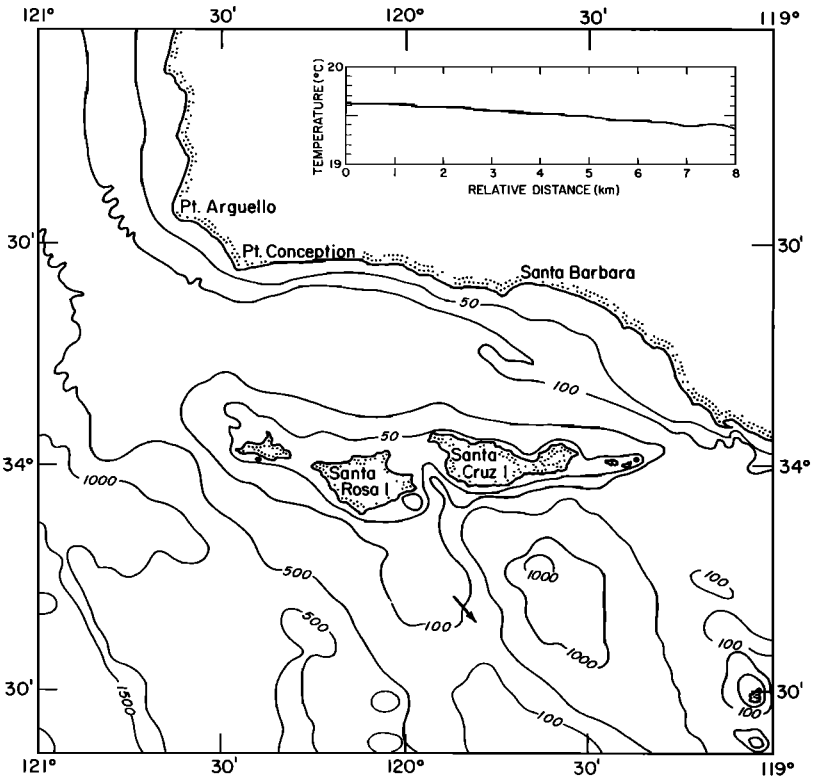

Fig. 1. Experimental location off the southern California coast showing ship track (arrow) in relation to Point Conception and the channel islands. Depth contours are in fathoms (1 fathom = 1.83 m). The inset shows sea surface temperature along the ship track.

Water within the averaging volume is thermally stratified, and the rate of irreversible kinetic energy loss due to mixing of local density gradients is computed.

2. Experimental Description and Data Processing

Data of this paper were collected during an engineering test of a microconductivity instrument between 2020 and 2150 PDT on October 24, 1983 southeast of Santa Rosa Island which lies off the southern California coast. The data section is located over the western sill of the Santa Cruz basin and consists of 24 profiles of temperature, conductivity, and pressure recorded during tow-yo profiling and include both upcasts and downcasts in an effort to maximize horizontal resolution. For 21 of the profiles microconductivity data were also obtained and were used to map the temperature microstructure field. The 8-km ship track in relation to the channel islands including Santa Rosa Island and Point Conception is shown in Figure 1; the direction and length of the ship track are indicated by an arrow. Water depth along the ship track varies from 150 m to 370 m. At the time of the experiment the wave height was about 1 m with a steady wind of 3.6 m s^{-1} from 330°. The primary instrumentation used during the experiment consists of a Neil Brown conductivity-temperature-depth probe (CTD) and a microconductivity instrument mounted on a tow-yo platform. For these data the average platform speed is about 1.45 m s^{-1}, and the towing angle with respect to the horizontal is about 18° on upcasts and 29° on downcasts. In the surface mixed layer, which extended to 16 m, there was a weak horizontal temperature gradient of 0.035°C km^{-1} along the ship track as shown in the sea surface temperature plot which is inset in Figure 1. Sea surface temperature was obtained by pumping water from a depth of about 2 m through a small chamber containing a platinum resistance thermometer.

Times series of temperature, conductivity, and pressure from the CTD are initially recorded at a 32-Hz sampling rate, smoothed with a 1-s running mean filter, and subsampled to a point every 0.5 s. To match the responses of the conductivity and temperature sensors, the conductivity time series is low-pass filtered before averaging with a one-pole digital filter with an effective analog time constant of 100 ms. These smoothed time series are used to compute salinity and density. Vertical gradients of temperature (used in computing Cox numbers), salinity, and density (used in computing the buoyancy frequency) are obtained by further smoothing the 1-s averaged time series with a 4-bar running mean filter. Vertical gradients are then computed from a first difference between adjacent points of these pressure-averaged time series. For these data, averaging over 4 dbar was found to be a reasonable compromise between vertical resolution and minimizing effects of spiking in profiles of the salinity and density gradients. In some regions of step and layer fine structure, however, vertical gradients of temperature,

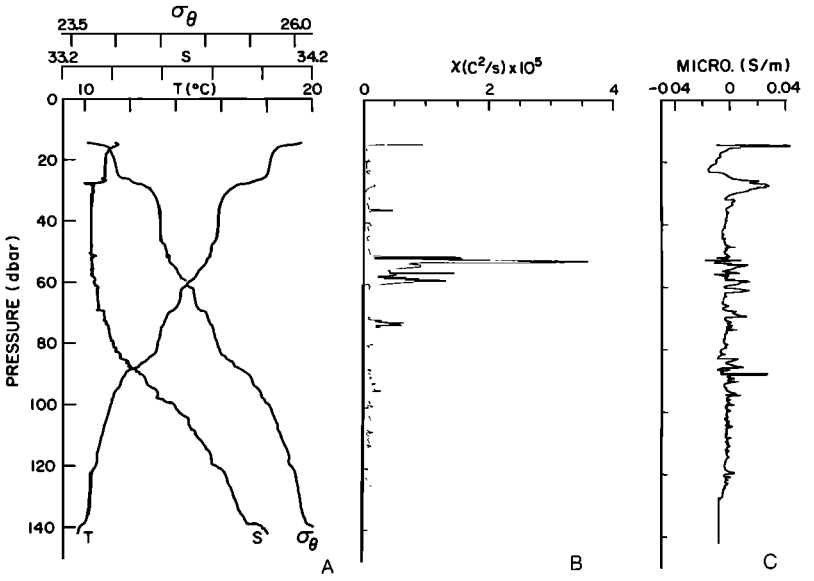

Fig. 2. (a) Profiles of temperature, salinity, and potential density anomaly for profile 4. (b) Temperature variance dissipation rate χ for profile 4. (c) Microconductivity signal for profile 4.

salinity, and density will be underestimated. At sea the microconductivity and CTD data streams are recorded separately and later merged through software during subsequent processing.

A primary microstructure quantity derived from measurement of conductivity is the local temperature variance dissipation rate $\chi = 2D\,\overline{(\partial T'/\partial x_i)^2}$ where T' is a temperature fluctuation and D is the thermal diffusivity of seawater (taken to be a constant of 1.40×10^{-7} m^2 s^{-1}); summation is over i=1, 2, and 3. Here the overbar denotes a volume average. Typically, in oceanic mixing events, χ is dominated by temperature gradients with wavelengths of less than 0.1 m. The response of the microconductivity probe used for measuring these small gradients has been measured in a laboratory water tunnel [Washburn and Deaton, 1986] and found to have a response closely corresponding to a one-pole spatial filter with a -3 dB wave number of 100 c m^{-1}. Because of the rather high noise level of these data, no correction for limited spatial resolution has been applied. In regions of strong microstructure activity, this results in χ being underestimated by as much as 50%, although typically the underestimate is much smaller. Conductivity is sampled at 512 Hz which corresponds spatially to a point about every 0.003 m along the tow-yo path. Estimates of χ are obtained from 1-s averages of $(dT'/dt)^2$ by using the Taylor hypothesis of frozen flow and assuming isotropy of the temperature fluctuations, $\chi=6D(1/\overline{U})^2(d\overline{T}'/dt)^2$, where $\overline{U}$ is the average platform velocity for the 1-s segment. The horizontal component of platform velocity is obtained from ship's position data, while the vertical component is computed by differentiating the pressure signal. These 1-s averages of χ are merged with the averaged CTD data by linear interpolation based upon time from a clock in the CTD which is initially recorded in both data streams. A more complete discussion of the instrumentation, platform velocity estimation, merging procedure, and data processing is given by Washburn and Deaton [1986].

In computing χ it is assumed that all of the conductivity gradient variance is due to temperature with no contribution from salinity fluctuations. As will be shown in section 3, this assumption is justified for these data above about 80 dbar where vertical salinity gradients are small. Minimum observed values of χ are about 7.0×10^{-7} $°C^2$ s^{-1} and are taken to be the effective noise level of the instrument system. This noise level is determined by the limited dynamic range of the audio tape recorder used in recording the microconductivity data. The focus of this paper is on the most active regions of the data record which are encountered repeatedly on successive upcasts and downcasts and which are well above the noise level.

3. Distribution of Mixing Activity

Figure 2 shows quasi-vertical profiles of temperature, salinity, and potential density anomaly σ_θ for profile 4, the first profile for which microstructure data were obtained. Based on the profile depth and the tow path angle, the horizontal distance traveled during this upcast is about 430 m; a horizontal distance of about 250 m is traversed during a typical downcast. The profiles of Figure 2 extend from the base of the surface mixed layer at 16 dbar to 140 dbar. Below 30 dbar both temperature and salinity gradients contribute to stable density gradients. Figure 2c gives the corresponding microconductivity profile in siemens per meter which has been high-pass filtered at 0.14 Hz, and because this is an upcast, temperature steps appear as local maxima in the signal as warmer water is encountered. Between 50 and 60 dbar in Figure 2c, regions of negative conductivity change are evident which signify the presence of temperature inversions and horizontal temperature gradients on scales of 0.5 m and smaller. The temperature

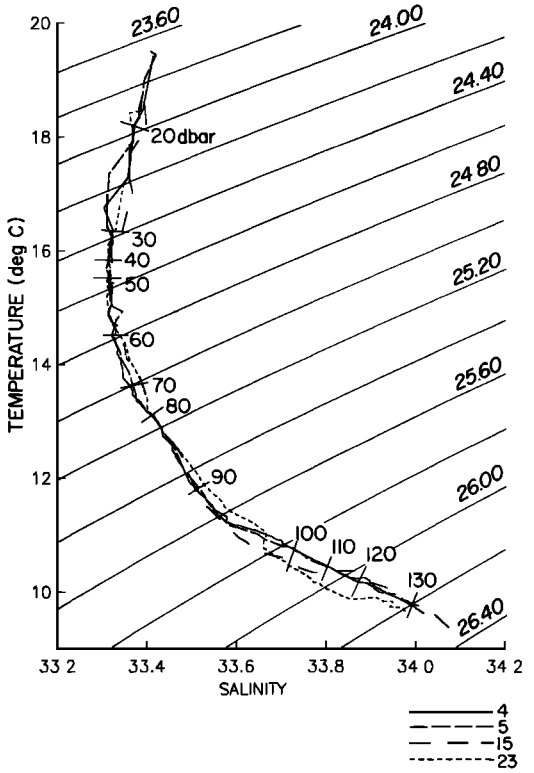

Fig. 3. T-S diagrams for profiles 4 (solid line), 5 (dashed line), 15 (dashed line, long space), and 23 (dotted line). Pressures are given for profile 4.

variance dissipation rate χ, shown in Figure 2b, rises abruptly in this depth interval with peak values exceeding 2.0×10^{-5} °C^2 s^{-1}. A second region of activity extending over 4 dbar may also be seen centered at 73 dbar.

Temperature-salinity (T-S) curves for one upcast and three downcasts, profiles 4, 5, 15, and 23, are shown superimposed in Figure 3. These profiles are spaced throughout the data record, and pressures for profile 4 are indicated in the figure. Except for a possible weak intrusion between isopycnals 25.80 and 26.10 of profile 23, thermohaline intrusions are absent in the section and the loci of T-S point for the profiles is fairly constant. Irregularities in the profiles between 20 and 60 dbar are due to salinity spiking in regions of high vertical temperature gradient which result from mismatch in the response times between the CTD conductivity and temperature sensors. Between 50 and 60 dbar the vertical salinity gradient is nearly zero, and thus for this depth interval which includes the events of Figure 2, temperature inversions must also be density inversions.

All σ_θ profiles for the entire data record are shown in Figure 4a; the σ_θ scale applies to the first profile and successive profiles are offset by 0.35. Profiles are numbered sequentially as shown at the top of the figure; even-numbered profiles are upcasts and odd-numbered profiles are downcasts. Midpoints of these profiles are separated on average by about 340 m. Pairs of dashed lines in Figure 4a, which bound regions of density fine structure, also bound regions of mixing activity as discussed below. The extent

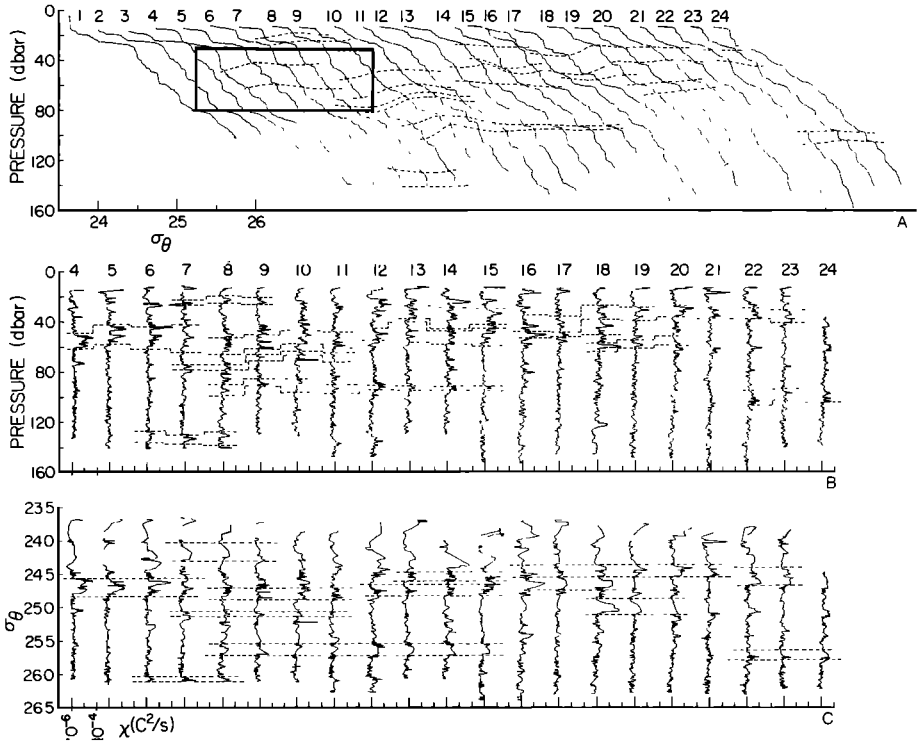

Fig. 4. (a) Potential density anomaly for all profiles. Successive profiles are offset by 0.35. Dashed lines correspond to isopycnals shown in Figures 4b and 4c. The rectangle shows the data section of Figure 5. (b) Plot of χ as a function of presssure for profiles 4 through 24. No microstructure data were obtained for profiles 1 to 3. Pairs of dashed lines indicate isopycnals containing regions of microstructure activity which extend among profiles. Successive profiles have been offset by 3 decades. (c) As in Figure 4b, but with χ plotted as a function of potential density anomaly.

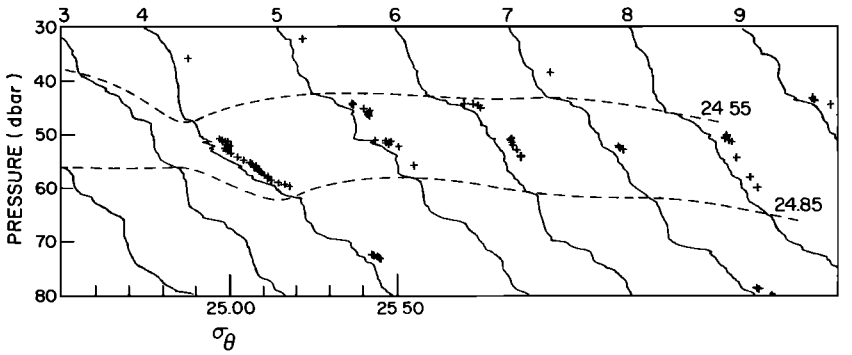

Fig. 5. Expanded portions of σ_θ profiles 3 through 9. Profiles are offset by 0.35. Plus signs mark portions of the profiles for which χ exceeds 3.0×10^{-6} °C^2 s^{-1}. Dashed lines indicate isopycnal surfaces 24.55 and 24.85. No microstructure data were obtained for profile 3.

of the surface mixed layer is evident in profile 1 above 16 dbar; all subsequent profiles stop below the mixed layer. Corresponding profiles of χ versus depth for a subset of the section covering a horizontal distance of about 6.7 km are shown in Figure 4b. No microstructure data were obtained for the first three profiles. The scale for χ is indicated for the first profile in Figure 4c and successive χ profiles are offset by 3 decades. Gaps in some profiles (profile 7 at 18 dbar, for example) result from clipping of the microconductivity signal in regions of large vertical temperature gradient. When the clipping occurs in the data, the signal is briefly held off scale and constant, which results in zero values of variance (and χ). In computing mean values and in producing contour plots, segments containing clipped regions were replaced with the observed modal value of the χ distribution. The occurrence of these clipped regions in the data is very infrequent, and their effects on the results are negligible. Regions of high χ are generally thinner than 5 dbar, although a few are as thick as 10 dbar such as in profiles 4 and 5 above 60 dbar. Dillon [1982] reports regions of $\chi > 10^{-5}$ °C^2 s^{-1} with comparable vertical extents at the base of the mixed layer and below from ocean station P during the Mixed Layer Experiment (MILE). Pairs of dashed lines in Figure 4b mark the depths of isopycnals bounding regions of microstructure activity which may be traced from profile to profile. Vertical displacements of isopycnals due to internal waves show some vertical coherence (profiles 8, 9, 10, and 11 between 50 and 85 dbar) and may be as large as 12 dbar (between profiles 17 and 18 at 35 dbar).

The same profiles are plotted as functions of σ_θ in Figure 4c with the same pairs of isopycnals of Figure 4a and 4b shown with dashed lines. Irregularities in some profiles near the surface (profile 15, for example) are due to density spikes which result from vertical velocity reversals of the instrument platform in high gradient regions. When plotted with the density ordinate, several mixing regions within the dashed lines are clearly seen to lie along isopycnal surfaces and have isopycnal extents up to several hundred meters. Mixing regions which occur on high density gradients are stretched when plotted versus σ_θ as in profile 18 at 60 dbar or σ_θ of 25.00. Within bands of isopycnals the detailed vertical structure of χ varies considerably from profile to profile and may result from modulation of mixing events by local fine structure on vertical scales of a few meters and smaller. This may also indicate that mixing regions of high average values of χ are composed of individual events with isopycnal extents which are smaller than the profile spacing. The occurrence of numerous mixing events in "clouds" or "clusters" with horizontal scales of 20 m and smaller has been reported by Washburn and Gibson [1984] in the seasonal thermocline.

A detailed view of part of eight σ_θ profiles beginning with profile 3 is given in Figure 5 and includes the region of strong activity between the σ_θ surfaces 24.55 and 24.85. This subsection of data is indicated by the rectangle in Figure 4a and covers a horizontal distance of about 2400 m. Portions of the profiles for which $\chi > 3.0 \times 10^{-6}$ °C^2 s^{-1} are indicated by plus signs to the right of each profile and comprise 4.8% of the total record. In Figure 5 where strong mixing activity is indicated by the microconductivity instrument, inversions are also evident in some portions of the σ_θ profiles obtained from the CTD (profile 4 at 52 dbar and profile 5 at 50 dbar, for example), although these are not completely resolved by the CTD temperature and conductivity sensors.

To better examine the spatial distribution of mixing activity, a two-dimensional map of log χ as a function of pressure is shown in Figure 6a. In producing the map, data of Figure 4b were smoothed with a 16-point running mean filter (8-s average) and subsampled by a factor of 8, giving a smoothed χ value about every 5 m along the tow path. The tow path followed by the profiler is shown in Figure 6a as a dashed line which crosses up and down across the contour plot. The depth range in Figure 6a of 15 to 120 dbar is chosen for the mapping region because this range is sampled by all microstructure profiles. The contour interval of the map is 0.2 in log χ with a minimum contour values of -6. Regions for which log $\chi > -5.8$ corresponding to $\chi > 1.6 \times 10^{-6}$ °C^2 s^{-1} are shown by stippling. A principal feature of the map is a band of strong mixing activity extending about halfway across the region between 40 and 60 dbar. The horizontal extent of this region is not completely covered by the survey, but must exceed the 2.6 km indicated in the figure. The aspect ratio of this region, therefore, is larger than 130. A second region of activity slopes downward at an angle of about 1.2° from 23 to 64 dbar between

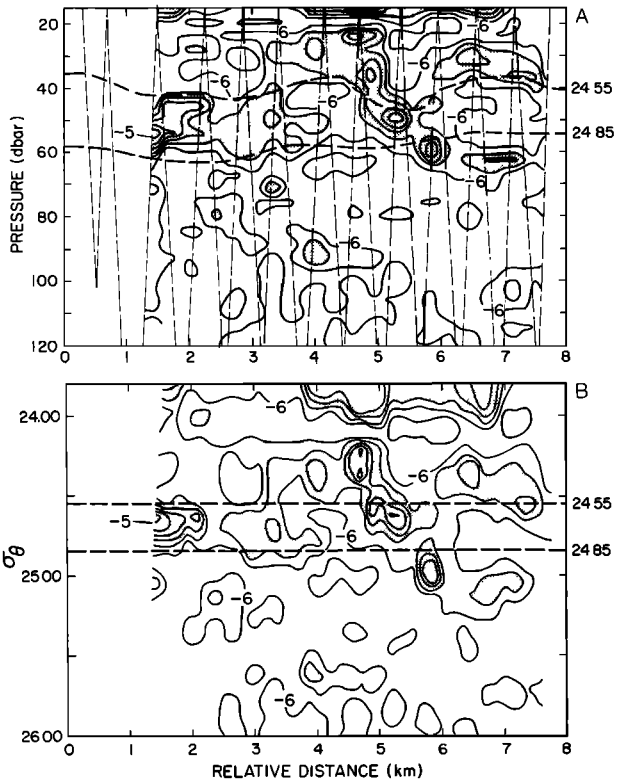

Fig. 6. (a) Distribution of χ in the pressure-distance coordinate system. Stippled areas indicate regions where χ exceeds 1.58×10^{-6} $°C^2\ s^{-1}$. Heavy dashed lines indicate isopycnal surfaces σ_θ=24.55 and 24.85. The tow path is indicated by the light dashed line. (b) As in Figure 6a, but for χ distribution in the σ_θ-distance coordinate system.

about 4.1 and 6.1 km. Mixing activity at the base of the mixed layer is indicated by $\chi > 1.6 \times 10^{-6}$ $°C^2\ s^{-1}$ between 1.5 and 1.9 km and between 3.9 and 7.0 km at the top of the figure. A few scattered regions of elevated mixing activity below 70 dbar may also be seen, although for most of this area, signals are very nearly at the noise level. The same data contoured as a function of σ_θ are shown in Figure 6b with the range of σ_θ corresponding approximately to the pressure range of Figure 6a. The region of strong mixing activity between 40 and 60 dbar centered at about 1 km is seen to collapse between the 24.50 and 24.80 σ_θ surfaces. Strong activity at the base of the surface mixed layer which occurs between 3.9 and 7.0 km is more prominent in this map because it occurs within a large density gradient and is stretched vertically. While many of the mixing events tend to be along isopycnals as shown in Figure 4, some events such as the one in profile 15 between 38 and 55 dbar lie across isopycnals. This is seen more clearly in Figure 6b as a region of elevated microstructure activity centered at about 4.8 km which slopes downward to the right. Similar observations of mixing events lying both along and across isopycnals are reported by Dugan [1984] through mapping of small-scale temperature variance (rather than χ). The isopycnal extent of mixing activity in Figure 6b is largest near the base of the surface mixed layer, about 3 km, and decreases to 2 km or less below. Deeper in the record the observations indicate a much shorter decorrelation length for the most active events consistent with an overall decrease in microstructure activity with depth.

4. Diapycnal Heat Transport and Energy Dissipation

In this section the spatial distributions of microstructure quantities within a specific averaging volume are considered in detail in order to estimate which terms are important in the budget equation for small-scale temperature variance. While no corresponding velocity measurements were made to directly estimate the production and advective terms in the budget, it is possible to establish lower bounds on typical velocities for these terms which are required to separately balance the measured dissipation within the averaging volume. The requirement of a very large velocity in a particular balance suggests that the balance is not possible and that the particular term is not important in the variance budget. In this case the comparison of the various terms leads to the familiar balance first proposed by Osborn and Cox [1972] and results in an estimate of the average diapycnal eddy diffusivity for the averaging volume.

The budget equation for temperature variance $(T')^2$ may be written as (see Gargett [1984] or Dillon [1984])

$$\frac{\partial}{\partial t}\overline{(T')^2} = -\frac{\partial}{\partial x_i}\overline{u_i(T')^2} - 2\overline{u_i T'}\frac{\partial \overline{T}}{\partial x_i} - \overline{\chi} \quad (1)$$

where u_i is the velocity, T' is a temperature fluctuation, χ is defined in section 2, and $i = 1$, 2, and 3 with the $i=3$ axis positive upwards. Overbars indicate a volume average. For these data, microstructure quantities are mapped in two dimensions, and variability at right angles to the data section ($i=2$ axis) is neglected; summation is over $i=1$ and 3. If, on the other hand, it is assumed that horizontal variability is isotropic, then contributions by the horizontal advection and production terms would have to be multiplied by a factor of 2 in the following analysis. The last term and the mean temperature gradients along the $i=1$ and 3 axes in the second term on the right-hand side of (1) may be estimated from a two-dimensional mapping of temperature microstructure. In addition, the spatial gradients $\partial\overline{(T')^2}/\partial x_i$ in the x_1 and x_3 directions may also be estimated from these observations. Following Gargett and Holloway [1984], no separation of the velocity field into mean and fluctuating components based upon a separation of length scales is made at this point.

A distinction which is made here in evaluating (1) is identifying that portion of the temperature variance which results from mixing processes. In the analysis below, temperature variance is composed of temperature fluctuations with wavelengths of about 1.5 m and smaller as measured along the tow path. In regions with little or no mixing activity, temperature variance at these scales results primarily from local temperature fine structure and is not

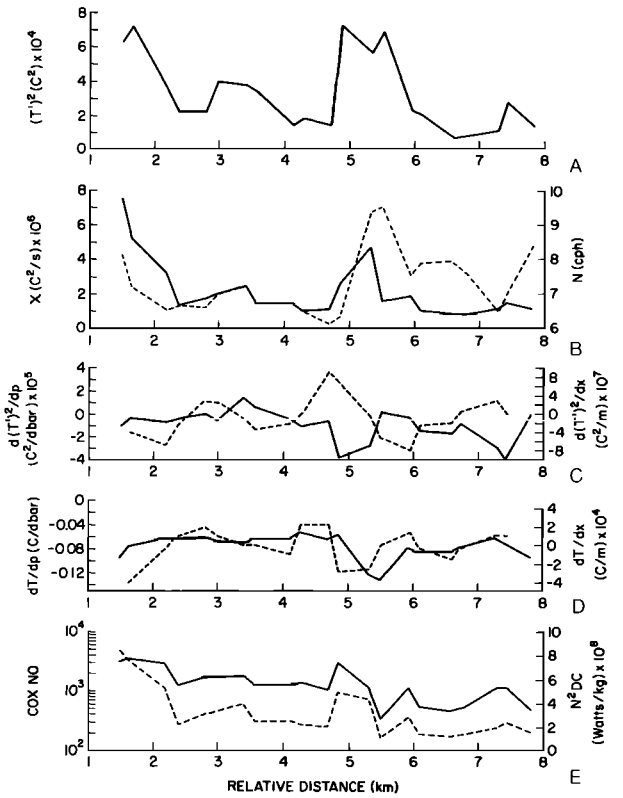

Fig. 7. Profiles of the following quantities averaged between σ_θ surfaces 24.55 to 24.85: (a) Temperature variance $(T')^2$. (b) Temperature variance dissipation rate (solid line) and buoyancy frequency N (dashed line, scale at right). (c) Diapycnal (solid line) and isopycnal (dashed line, scale at right) gradients of $(T')^2$. (d) Diapycnal (solid line) and isopycnal (dashed line, scale at right) mean temperature gradients, and (e) Cox number (solid line) and available potential energy dissiptation rate (dashed line, scale at right) N^2DC.

necessarily directly related to mixing processes. However, for regions of strong mixing activity (high values of χ) which are the focus of this section, temperature variance at these scales is found to be correlated with χ, which indicates that most of the observed variance in these regions is the result of mixing activity.

The volume selected for estimating terms in (1) is bounded vertically between the σ_θ surfaces 24.55 and 24.85; the length of the region is about 6.7 km with an average height of about 17 m. The height of the volume was chosen to be larger, on average, than the most active mixing regions. The i=1 and i=3 axes are in the isopycnal and diapycnal directions, respectively. This region was selected because signals are well above the noise level and transits through the region are approximately spaced uniformly, as may be seen in Figure 6a. The distribution of mixing activity with respect to this volume may be seen in Figure 6; the averaging volume is indicated by dashed lines which run horizontally across the figure. Computing averages between σ_θ surfaces rather than between fixed depths is suggested by the collapse of mixing regions onto σ_θ surfaces evident in Figure 4. Furthermore, fixing the volume to isopycnal surfaces reduces the possible vertical advective contributions to the variance budget from internal waves and better separates the diapycnal mixing processes.

The profile of $(T')^2$ across the averaging volume is shown in Figure 7a and the corresponding profiles of χ (solid line) and N (dashed line) are shown in Figure 7b. Profiles of $\partial T/\partial p$ and $\partial(T')^2/\partial p$ are shown with solid lines in Figures 7c and 7d, respectively; profiles of $\partial T/\partial x_1$ and $\partial(T')^2/\partial x_1$ are shown with dashed lines in these figures. All points in the profiles of Figure 7 represent averages between σ_θ=24.55 and σ_θ=24.85 for each transit through the averaging volume. The isopycnal profiles of $(T')^2$ and χ in Figures 7a and 7b are found to be significantly correlated (r^2=0.52) at a 95% confidence level, while N and χ were found to be uncorrelated (r^2=0.08). Mean values and standard deviations of the seven quantities of Figures 7a, 7b, 7c, and 7d averaged over the width of the isopycnal band are listed in Table 1. For this region the mean value of the diapycnal temperature gradient is about 7000 times the isopycnal gradient; the mean diapycnal gradient of $(T')^2$ is about 100 times the isopycnal gradient.

The diapycnal distributions of fine structure and microstructure quantities averaged over the width of the section are shown in Figure 8. An estimate of the fraction of each isopycnal surface which contains strong mixing activity ($\chi > 1.6\times10^{-6}$ °C^2 s^{-1}) is given in Figure 8a and is obtained graphically from the map of Figure 6b. Error bounds are determined by superimposing the tow path over the map and assuming (1) for the lower bound, that the activity extended only between consecutive profiles for which χ exceeded the threshold value given above and no further or (2) for the upper bound, that activity extended to the next consecutive profile which had activity less than the threshold. Figure 8a indicates that for isopycnal surfaces near the base of the mixed layer, over half of a given surface contains strong activity. This may be an underestimate since some clipping of signal levels occurred in the high temperature gradients encountered at the mixed layer base. The averaging volume used below in estimating terms in the temperature variance budget falls in a portion of the profile where the fraction of activity is decreasing with increasing density;

TABLE 1. Mean Values Averaged Between σ_θ=24.55 and 24.85.

Parameter	Value
χ, °C^2 s^{-1}	$(2.2 \pm 1.7) \times 10^{-6}$
N, cph	7.33 ± 0.94
$(T')^2$, °C^2	$(3.3 \pm 2.2 \times 10^{-4}$
$\partial T/\partial x$, °C m^{-1}	$(-1.1 \pm 17.5) \times 10^{-5}$
$\partial T/\partial p$, °C dbar^{-1}	$(-7.7 \pm 2.0) \times 10^{-2}$
$\partial(T')^2/\partial x$, °C^2 m^{-1}	$(-6.4 \pm 43.1) \times 10^{-8}$
$\partial(T')^2/\partial p$, °C^2 dbar^{-1}	$(-9.9 \pm 14.0) \times 10^{-6}$
p, dbar	49.3 ± 6.3
Δp, dbar	16.8 ± 3.3
$\dot{p} = N^2DC$, W kg^{-1}	$(3.1 \pm 2.0) \times 10^{-8}$
C	1436 ± 885

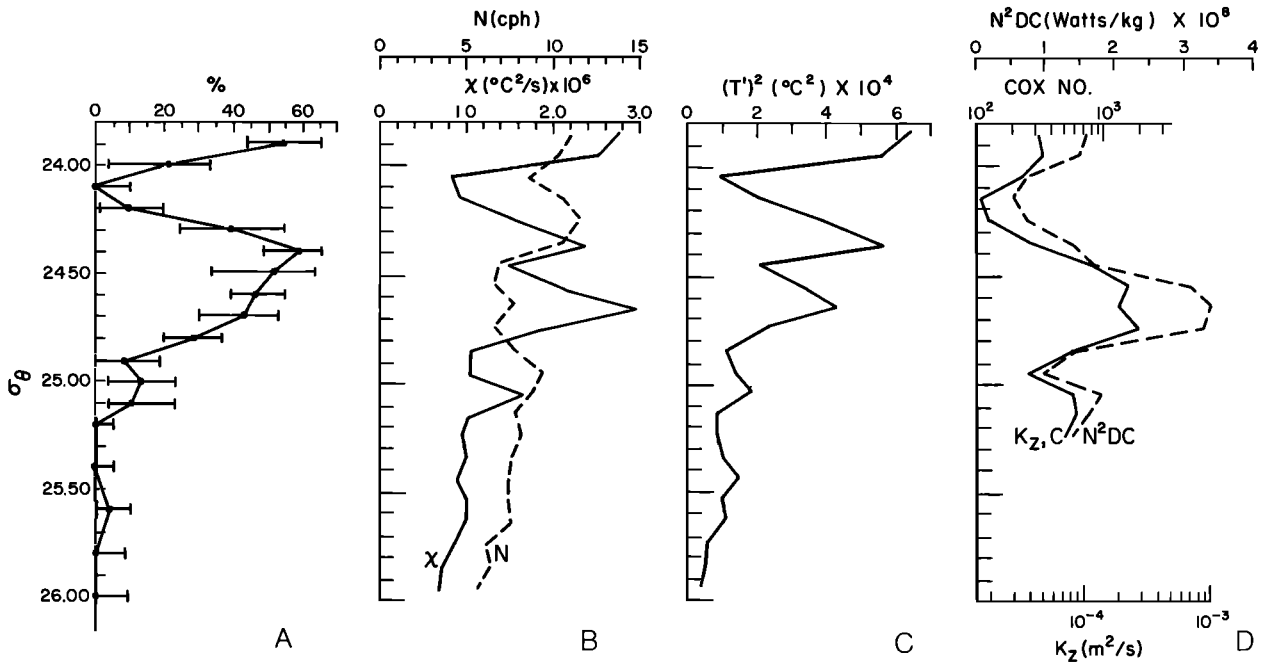

Fig. 8. (a) Fraction of isopycnal surfaces containing regions of strong mixing activity ($\chi > 1.58 \times 10^{-6}$ °C^2 s^{-1}) obtained from map of Figure 6b. (b) Diapycnal profiles of χ (solid line) and N (dashed line) averaged over σ_θ intervals of 0.10. (c) As in Figure 8b but for diapycnal profile of $(T')^2$. (d) As in Figure 8b but for diapycnal profiles of Cox number C (solid line) and N^2DC (dashed line). The scale for K_z is given at bottom.

about half of the upper surface (σ_θ=24.55) contains strong mixing activity while only about 15% of the lower surface (σ_θ=24.85) does. Figure 8b shows diapycnal profiles of χ (solid line) and N (dashed line) which have been averaged over σ_θ intervals of 0.10, and Figure 8c shows the corresponding profile for $(T')^2$. Each point in the isopycnal χ and $(T')^2$ profiles of Figures 8b and 8c is typically composed of about 450 1-s averages. Some features of the χ profile are evident in the profile of $(T')^2$, and the two profiles are found to be significantly correlated (r^2=0.77), indicating that most of the observed variance is the result of mixing activity. No significant correlation is found between χ and N (r^2=0.01) for the diapycnal profiles of Figure 8b.

From a comparison of Figures 7a and 7b and Figure 8b and 8c it is found that χ represents a strong sink for $(T')^2$ in (1), and if a stationary balance is to be maintained, an equally strong net source must exist on the right-hand side or variance must be transported into the averaging volume at a rate which will sustain the observed dissipation. If no source of $(T')^2$ exists in the averaging volume or if transport is insignificant, the average value of χ will deplete $(T')^2$ in a time τ which is less than the average buoyancy period N^{-1}, $\tau = (T')^2/\chi = 0.3$ N^{-1} based on the average values of Table 1. A qualitatively similar result has been reported by Dillon [1982] for mixing events in the surface mixed layer and seasonal thermocline during MILE, although his estimate of the time scale for $(T')^2$ depletion for several individual microstructure patches is even smaller, in the range of about 0.16 to less than 0.016 N^{-1}. Part of the difference between the two estimates depends upon the definition of $(T')^2$ and the way in which the data are averaged. Here $(T')^2$ is computed from temperature fluctuations with wavelengths of 1.5 m and smaller as discussed above, and averages are computed between fixed isopycnals. Dillon [1982] computed $(T')^2$ from the measured profile minus a profile which is monotonic in density (used for computing the "Thorpe scale") and took averages through individual events. Regardless of the definition, these decay time estimates indicate that temperature variance within mixing regions at microstructure scales is a very volatile quantity. The period of time over which the averaging volume was observed is about 1.4 h or about 35 times greater than the time scale for variance depletion within the volume. This means that variance must have been created within or transported into the averaging volume over the period of observations and is at least consistent with an assumption of steady state in the level of $(T')^2$ within the volume.

Because only a single two-dimensional section is available from the experiment it is not possible to be certain that the average level of $(T')^2$ is not changing in time. However, the averaging volume is large enough to contain a number of regions of mixing activity, and the overall temporal variation of $(T')^2$ results from their combined evolution. Selection of relatively large averaging volumes increases the likelihood that mixing regions will be encountered in various states of evolution; i.e., some will be "growing" $\partial(T')^2/\partial t > 0$, while others will be "decaying" $\partial(T')^2/\partial t < 0$. It

seems likely that for large volumes such as this one which enclose several mixing regions, the sum of the individual contributions will tend to approach zero and the average level of $(T')^2$ will approach steady state. However, temporal variability in the large scale flow field which drives the mixing processes within the volume could result in variability in the average level of $(T')^2$ on a comparable time scale. The relatively short time scale for $(T')^2$ depletion suggests that local production of $(T')^2$ will dominate the contributions from the advective terms in (1) for the averaging volume considered here.

An estimate of a mean velocity along each axis required to separately produce a balance between the observed distribution of χ within the averaging volume and mean advection of $(T')^2$ into the volume may be obtained by setting the first and last terms on the right-hand side of (1) equal to each other and solving for for a spatially constant $u_i=U_i$,

$$U_i = - \frac{\bar{\chi}}{\partial (T')^2/\partial x_i} \qquad (2)$$

Conversion of pressure derivatives to vertical spatial derivatives is done by assuming that +1 dbar equals -1 m. Using the mean values from Table 1, these velocity estimates are velocity estimates are 34 m s^{-1} and -0.22 m s^{-1} for U_1 and U_3, respectively, and are unrealistically large. For comparison, vertical velocities in active upwelling regions off northern California are in the range $1.2\text{-}3.6\times10^{-4}$ m s^{-1} (10-30 m d^{-1}) as reported by Lentz [1987], some 3 orders of magnitude less than this estimate of U_3. The much larger isopycnal mean velocity required is due in part to the much larger isopycnal dimension of the averaging volume: the high aspect ratio averaging volume is chosen to examine diapycnal mixing processes.

A similar balance between the first and last terms on the right-hand side of (1), but allowing u_i to be spatially variable, yields the flux divergence of $(T')^2$ required to equal the observed dissipation. Using Gauss' theorem, the balance between flux divergence and dissipation within an averaging volume may be expressed as

$$\int_\Sigma (T')^2 u_i n_i d\sigma = - \int_V \chi dv$$

where n_i is a unit vector normal (positive outwards) to the surface Σ which enclosed the volume V. Defining a correlation function c_2 between $u_i n_i$ and $(T')^2$ on Σ,

$$\int_\Sigma (T')^2 u_i n_i d\sigma \equiv c_2 (T')^2_{rms} u_{rms} \Sigma$$

leads to an estimate of the rms velocity normal to Σ,

$$u_{rms} = \frac{\bar{\chi} H}{c_2 (T')^2_{rms}} \qquad (3)$$

For the high aspect ratio averaging volume ($L/\Delta x_3=400$) considered here, the length $H=V/\Sigma$ is approximately $\Delta x_3/2$, where Δx_3 is the average diapycnal dimension of the averaging volume (17 m).

Assuming u_i and $(T')^2$ to be perfectly correlated, $c_2=-1$, so that $(T')^2$ is transported inward through Σ everywhere, and using the mean values from Table 1, a lower bound on the required u_{rms} into the volume at the boundary is about 0.06 m s^{-1}. While this is not an unreasonably large velocity estimate, actual instantaneous velocities on the boundary would have to be much larger because not all of the boundary contains strong mixing activity and high variance levels as shown in Figure 8a. Furthermore, by continuity, the integral of $u_i n_i$ over Σ is zero and it seems unlikely that $(T')^2$, a positive definite quantity, will be large only in those areas of Σ where u_i is inward. To satisfy inward transport of $(T')^2$ everywhere on Σ as is assumed above, high values of $(T')^2$ would have to be correlated with negative (downward) velocities on the upper isopycnal boundary and at the same time be correlated with positive (upward) velocities on the lower boundary. This would imply that basically different physical processes are operating on the two boundaries inasmuch as the sense of the correlation between diapycnal velocity and $(T')^2$ is different. If, on the other hand, the same basic processes are operating on both boundaries so that diapycnal velocity and $(T')^2$ are correlated in the same sense, then transport of $(T')^2$ out of Σ would occur in some areas and the magnitude of c_2 would be reduced. This would increase the required velocity estimate given by (3). In considering this balance between advection and dissipation, no specific process such as internal waves or turbulence, for example, is specified, and no separation of the velocity field into mean or fluctuating components has been made.

Equating the last two terms on the right-hand side of (1) yields the internal production of $(T')^2$ required to balance the observed dissipation. Solving for $\overline{u_i T'}$,

$$\overline{u_i T'} = - \frac{\bar{\chi}}{2\, \partial \bar{T}/\partial x_i} \qquad (4)$$

By introducing the usual temperature velocity correlation function,

$$c_1 \equiv \frac{\overline{u_i T'}}{u_{i\ rms}\ T'_{rms}} \qquad (5)$$

the required rms velocity may be written as

$$u_{i\ rms} = - \frac{\bar{\chi}}{2 c_1 T'_{rms}\ (\partial \bar{T}/\partial x_i)} \qquad (6)$$

Again, a lower bound on an velocity may be estimated by assuming perfect correlation between u_i and T'. Taking $c_1=1$ and using mean values from Table 1 results in an estimate of an rms diapycnal velocity $u_{3\ rms}$ of 0.0008 m s^{-1} from (6) and an rms isopycnal velocity $u_{1\ rms}$ of 5.3 m s^{-1} which is unrealistically large. The correlation function c_1 has never been measured in oceanic mixing events at dissipative scales,

but its magnitude is surely less than 1. Stillinger et al. [1983] have measured the correlation function $\overline{(\rho'w')}/(\rho'_{rms}w'_{rms})$ for grid-generated turbulence in a stratified water tunnel for three values of N (0.45, 0.73, and 0.95 rad s^{-1}) and found peak values of c_1 of about 0.4. Here ρ' and w' represent density and vertical velocity fluctuations, respectively. More recently, Itsweire et al. [1986] report laboratory measurements of this correlation function over a wider range of stratifications (0.24 to 0.98 rad s^{-1}) with similar peak values. Itsweire et al. [1986] also found that the grid-generated turbulence was completely fossilized (in the sense that $\rho'w' = 0$) after about one quarter of a buoyancy period. All values of the stratification in these laboratory experiments were 1 to 2 orders of magnitude larger than typical maximum stratifications found in the seasonal thermocline. No consistent trends between N and either peak values of c_1 or decay times were apparent in the laboratory results, however. Using a peak value for c_1 of 0.4 from the laboratory experiments in (6) increases the estimate of $u_{3\ rms}$ to about 0.002 m s^{-1}, although this still probably represents a lower bound on a typical rms velocity. Nevertheless, the order of magnitude, rms velocity estimates developed above indicate that the most probable balance in (1) within this volume is between local diapycnal production and dissipation of $(T')^2$ which is, of course, the balance suggested by Osborn and Cox [1972]. It should be pointed out that the velocity estimates (2), (3), and (6) depend on complete resolution of χ, and in regions where χ is underestimated because of spatial resolution limitations, these will also be underestimated since χ always appears in the numerator. The ratios of the estimates will not be affected. The decay time τ, on the other hand, will tend to be overestimated.

An eddy diffusivity K_i may also be defined as

$$K_i \frac{\partial \overline{T}}{\partial x_i} \equiv - \overline{u_i T'} \qquad (7)$$

and if diapycnal production and dissipation balance, K_3 may be expressed as

$$K_3 = \frac{\overline{\chi}}{2(\partial \overline{T}/\partial x_3)^2} \qquad (8)$$

Substituting for χ in (8) yields the Cox number which gives the vertical eddy diffusivity of heat normalized by the thermal diffusivity of sea water.

$$C \equiv 3 \frac{\overline{(\partial T'/\partial x_m)^2}}{(\partial \overline{T}/\partial x_3)^2} \qquad (9)$$

In (9), x_m is in the direction of measurement with no summation on m. Cox numbers for all points in the isopycnal band σ_θ=24.55-24.85 are computed from 1-s averages of $(\partial T'/\partial x_m)^2$ (covering about 1.45 m along the tow path) using (9) where $(\partial \overline{T}/\partial x_3)^2$ is obtained from the smoothed temperature gradient profiles as was discussed in section 2. For each of the 21 transits through the σ_θ=23.55-23.85 isopycnal band, all values of C for each transit are averaged together and plotted as a function of horizontal position. A plot of C versus horizontal position is given in Figure 7e (solid line) and ranges between about 300 and 3300 with an average value of 1436 and a standard deviation of 885. This average Cox number corresponds to a diapycnal eddy diffusivity K_3 of 2.0×10^{-4} m^2 s^{-1}. Each point in Figure 7e is typically composed of about 70 individual values of the Cox number. Computed Cox numbers will be overestimates in thin, high gradient regions where $(\partial \overline{T}/\partial x_3)$ is underestimated due to smoothing. However, the resulting errors over the entire section are probably not too severe since a consistent trend for mixing events to occur only in the thinnest, high gradient regions, where underestimation of $(\partial \overline{T}/\partial x_3)$ is greatest, is not observed for these data. Figure 8d (solid line) shows the Cox number as a function of σ_θ averaged as in Figures 8b and 8c. A scale for K_z ($\equiv K_3$) is given at the bottom of Figure 8d assuming that the balance between diapycnal production and dissipation of $(T')^2$ holds for all isopycnal bands.

The choice of averaging volume is also important in determining which terms dominate the balance in (1). For small volumes which do not enclose mixing events, boundary fluxes of $(T')^2$ can be large. This is indicated explicitly in (3) by the presence of the length scale $H=V/\Sigma$; for small H, processes on the boundary can rapidly transport $(T')^2$ into the interior of an averaging volume, thus reducing the rms velocity fluctuation required to balance or exceed dissipation. For small H the balance in (1) could shift to one mainly between advection and time rate of change of $(T')^2$. Equating the velocity estimates (3) and (6), which is equivalent to equating the production and advective terms in (1), yields the length H of an averaging volume within which contributions from boundary fluxes and internal production are of the same order,

$$H = \frac{c_2}{c_1} \frac{T'_{rms}}{\partial \overline{T}/\partial x_i} \qquad (10)$$

In (10) the length scale given by the quotient of an rms temperature fluctuation and the mean temperature gradient can be interpreted as a vertical turbulent eddy scale if the internal wave contributions to T'_{rms} are small [Caldwell, 1983] and if variance is not produced by horizontal mixing, i.e., $x_i = x_3$ in (10). This interpretation is probably valid for these data because temperature variance for the range of length scales examined is found to be correlated with mixing activity (χ) and isopycnal temperature gradients are small in the region. As discussed by Itsweire et al. [1986], this vertical overturning scale, which they call L_t, is smaller than the Thorpe scale by a factor of about 1.2 for grid generated turbulence in the laboratory. This length scale is multiplied by the ratio (c_2/c_1) which indicates the relative efficiency of transport of variance into the averaging volume compared to the rate of production of variance internally. The scale H

gives a measure of the vertical resolution of the Osborn and Cox [1972] model; certainly direct measurements of the correlation functions, c_1 and c_2, in a wide variety of flows and over a broad range of wave numbers are required to establish it precisely. Taking average values from Table 1 and assuming that c_1 and c_2 are of the same order, the diapycnal dimension of a high aspect ratio averaging volume from (10) is about H=0.2 m. The thickness of the volume between σ_θ surfaces 24.55 and 24.85 is about 70 times this value, and because the volume encloses many mixing events both along and across isopycnals, boundary flux contributions are reduced. This length scale estimate is also within the range of wavelengths for which fully developed turbulence can exist within typical mixing events in the averaging volume, as will be discussed in the next section. Transport of $(T')^2$ by turbulent eddies, therefore, is probably large and the advective term in (1) is important in the budget for $(T')^2$ at vertical scales of the order of 0.2 m and smaller.

Because the water is thermally stratified throughout the averaging volume, dissipation of temperature fluctuations also corresponds to dissipation of density fluctuations. This smoothing of density variance removes available potential energy from mixing events; motions driven by local buoyancy flux (conversion from potential to kinetic energy) are reduced as local density gradients are mixed. For thermally stratified waters, (1) can be expressed as an available potential energy equation [Dillon, 1984; Gargett and Holloway, 1984] with the quantity $\dot{p}=N^2DC$ giving the rate at which available potential energy is lost through mixing of the local mean density gradient. An isopycnal profile of $\dot{p}$ evaluated across the averaging volume is shown in Figure 7e (dotted line) and has a mean value of 3.1×10^{-8} W kg^{-1}. For comparison, a typical value for ε in the surface mixed layer is about 10^{-7} W kg^{-1} (see Gargett and Osborn [1981], for example), so this kinetic energy loss rate due to mixing of density gradients is substantial here. A diapycnal profile of $\dot{p}$, averaged as in Figure 8b and 8c, is shown in Figure 8d (dashed line) and is seen to have a maximum of 3.4×10^{-8} W kg^{-1} centered within the averaging volume. The ratio of $\dot{p}$ to ε is called the "mixing efficiency" [Gargett and Holloway, 1984; Oakey, 1982] $\Gamma \equiv \dot{p}/\varepsilon$ and represents the relative rate at which mixing events store kinetic energy through vertical mixing of local density gradients compared to the rate at which they dissipate kinetic energy into heat. Estimates of Γ from laboratory data [Osborn, 1980; McEwan, 1983] and oceanic microstructure data [Oakey, 1982; Dillon, 1982] typically scatter (widely) about a value of 0.25. For this region, therefore, $\dot{p}$ probably accounts for about 20% of the total rate of irreversible kinetic energy loss due to mixing activity.

5. Discussion and Conclusions

Temperature microstructure is mapped in two dimensions for a section 6.7 km long and about 150 m deep which is located on the continental shelf southeast of Point Conception on the southern California coast. Water in the section is free of thermohaline intrusions and above 80 m is thermally stratified. The distributions of temperature, salinity, density, and the buoyancy frequency N are mapped with a CTD, and the temperature variance dissipation rate χ is mapped with a microconductivity instrument which is mounted on the same tow-yo platform as is the CTD.

Mapping of χ in both pressure-distance and density-distance coordinate systems reveals that many mixing regions collapse onto isopycnal surfaces, although some regions lie across isopycnals. The isopycnal extent of one mixing region at the base of the surface mixed layer is about 3 km and the extent of another region, which is deeper in the record and which was not completely mapped, may be larger.

Terms in the budget equation for temperature variance $(T')^2$ are estimated for a volume 6.7 km long which is bounded vertically by isopycnal surfaces separated by 17 m on average. Within this volume, strong mixing regions are encountered repeatedly among upcasts and downcasts, and χ, averaged between the isopycnals bounding the volume, is above the noise level everywhere. Temperature variance $(T')^2$ is defined over a range of wavelengths of 1.5 m and smaller and is found to be correlated with χ, which indicates that $(T')^2$ is the result of small-scale mixing activity. Values of χ are sufficiently high that $(T')^2$ within the averaging volume is depleted in a time which is less than the local buoyancy period, a finding in agreement with observations of Dillon [1982]. This rapid depletion favors local production of $(T')^2$ in the budget equation compared with the advective contributions for the averaging volume considered here. By comparing each term in the budget equation against the observed levels of χ, the diapycnal production of $(T')^2$ is found to yield the most plausible balance. This is the balance proposed by Osborn and Cox [1972] and is consistent with an average diapycnal eddy diffusivity for heat of 2.1×10^{-4} m^2 s^{-1}.

The correlation noted between $(T')^2$, as defined, and χ is consistent with variance production by small-scale turbulent processes. The level of the observed average dissipation rate of available potential energy suggests that mixing processes are sufficiently energetic that small-scale, inertially dominated turbulence exists in the region. An order of magnitude estimate of ε for a "typical" mixing event within the volume can be made from the observed level of $\dot{p}=N^2DC$ and oceanic observations of the mixing efficiency Γ. Taking $\dot{p}$ from Table 1 and using $\Gamma \approx 0.25$ from Oakey [1982] yields $\varepsilon = \Gamma^{-1}\dot{p} \sim 10^{-7}$ W kg^{-1}. Laboratory [cf. Stillinger et al., 1983] and theoretical [cf. Gibson, 1980] investigations indicate that three-dimensional turbulence exists in a stratified fluid over a range of vertical wavelengths $AL_O > \lambda > BL_K$, where $L_O = (\varepsilon/N^3)^{1/2}$ is the buoyancy or Ozmidov length scale, $L_K = (\nu^3/\varepsilon)^{1/4}$ is the viscous or Kolmogorov length scale, ν is the kinematic viscosity of seawater ($\approx10^{-6}$ m^2/s), and A and B are constants. Values of A and B were predicted by Gibson [1980] to be 1.2 and 15, respectively, and were later measured in the laboratory by Stillinger et al. [1983] to be 1.4 and 15.5. Laboratory measurements of the cospectrum of $\rho'w'$ reported

by Itsweire et al. [1986] indicate that dominant contributions to the buoyancy flux (and production of $(T')^2$) result from this range of wavelengths, although they also observed significant buoyancy flux from wavelengths that are affected by viscosity. Substituting for A and B and using N from Table 1 gives a range of turbulent wavelengths 0.3 m $\geq\lambda\geq$0.03 m which is contained in the range of wavelengths contributing to $(T')^2$ and in which local production of $(T')^2$ due to small-scale turbulence would be expected to be large.

Holloway [1983, 1986a, b) has argued that values of $\overline{wT'}$ (and K_z) based upon the model of Osborn and Cox [1972] using temperature variance dissipation measurements are overestimates because of the neglect of the triple correlation terms in (1), which is equivalent to a spatial divergence $\partial/\partial x_i\ u_i(T')^2$. For the averaging volume considered here and the restricted range of wavelengths ($\leq$1.5 m) contributing to $(T')^2$, it is concluded that neglect of the triple correlation term in the $(T')^2$ budget is justified. The observed levels of χ represent such a strong sink for $(T')^2$ in this wave number range that transport of $(T')^2$ is ineffective over the scales of the chosen averaging volume. By defining $(T')^2$ over a range of wavelengths which is limited to that important in determining χ and by averaging over a volume which includes many mixing events, a balance between production and dissipation is, in a sense, selected for.

Acknowledgments. Helpful discussions were had with Laurence Armi, Tim Duda, Pierre Flament, Carl Gibson, David Siegel, Tom Dickey, and Alan Bratkovich. Sharon Yamasaki and Rick Olsen did much of the CTD data processing. Thanks to Walter Richter, Tim Boyd, Richard Williams, Vittorio Barale, and William Watkins for valuable assistance during data collection. Thanks also to Captain Tom Beattie and the crew of the Ellen B. Scripps throughout the experiment. This work was supported by the Office of Naval Research.

References

Caldwell, D. R., Oceanic turbulence: Big bangs or continuous creation?, J. Geophys. Res., 88(C12), 7543-7550, 1983.

Dillon, T. M., Vertical overturns: A comparison of Thorpe and Ozmidov length scales, J. Geophys. Res., 87(C12), 9601-9613, 1982.

Dillon, T. M., The energetics of over-turning structures: Implications for the theory of fossil-turbulence, J. Phys. Oceanogr., 14(3), 541-545, 1984.

Dugan, J. P., Towed observations of internal waves and patches of fine-scale activity paper presented at the Hawaiian Winter Workshop, Univ. of Hawaii at Manoa, Honolulu, January 17-20, 1984.

Gargett, A. E., Vertical diffusivity in the ocean interior, J. Mar. Res., 42, 359-393, 1984.

Gargett, A. E., and G. Holloway, Dissipation and diffusion by internal wave breaking, J. Mar. Res., 42, 15-27, 1984.

Gargett, A. E., and T. R. Osborn, Small-scale shear measurements during the Fine and Microstructure Experiment (FAME), J. Geophys. Res., 86, 1929-1944, 1981.

Gibson, C. H., Fossil temperature, salinity and vorticity turbulence in the ocean, in Marine Turbulence, edited by J. Nihoul, pp. 221-257, Elsevier, New York, 1980.

Gregg, M. C., H. Peters, J. C. Wesson, N. S. Oakey, and T. J. Shay, Intensive measurements of turbulence and shear in the equatorial undercurrent, Nature, 318, 141-144, 1986.

Holloway, G., A conjecture relating oceanic interval waves and small-scale processes, Atmos. Ocean, 21, 107-122, 1983.

Holloway, G., Do turbulence dissipation measurements imply ocean mixing? Ocean Model. 70, 1-3, 1986a.

Holloway, G., Considerations on the theory of temperature spectra in stably stratified turbulence, J. Phys. Oceanogr., 16(12), 2179-2183, 1986b.

Itsweire, E. C., K. N. Helland, and C. W. Van Atta, The evolution of grid-generated turbulence in a stably stratified fluid. J. Fluid. Mech., 162, 299-228.

Lentz, S. J., A description of the 1981 and 1982 spring transitions over the northern California shelf, J. Geophys. Res., 92(C2), 1545-1567, 1987.

McEwan, A. D., Internal mixing in stratified fluids, J. Fluid Mech., 128, 59-80, 1983.

Oakey, N. S., Determination of the rate of dissipation of turbulent energy from simultaneous temperature and velocity shear microstructure measurements, J. Phys. Oceanogr., 12, 256-271, 1982.

Osborn, T. R., Estimates of the local rate of vertical diffusion from dissipation measurements, J. Phys. Oceanogr., 10(1), 83-89, 1980.

Osborn, T. R., and C. S. Cox, Oceanic fine structure, Geophys. Fluid Dyn., 3, 321-345, 1972.

Stillinger, D. C., K. N. Helland, and C. W. Van Atta, Experiments on the transition of homogeneous turbulence to internal waves in a stratified fluid, J. Fluid Mech., 131, 91-122, 1983.

Washburn, L., and T. K. Deaton, A simple system for mapping conductivity microstructure, J. Atmos. Oceanic Technol., 3,(3), 345-355, 1986.

Washburn, L., and C. H. Gibson, Horizontal variability of temperature microstructure at the base of a mixed layer during MILE, J. Geophys. Res., 57(C3), 3507-3522, 1984.

L. Washburn, Ocean Physics Group, Center for Earth Sciences, University of Southern California, Los Angeles, CA 90089.

(Received December 26, 1986; accepted February 23, 1987.)